# An axon-T cell feedback loop enhances inflammation and axon degeneration

**Tingting Liu**[1,2,3], **Huanhuan Wang**[2,3], **Daniel Y. Kutsovsky**[1], **Michael Iskols**[1], **Hongjie Chen**[2], **Christine Y.J. Ohn**[1], **Nandan Patel**[1], **Jing Yang**[2], **David J. Simon**[1,4,*]

[1]Department of Biochemistry, Weill Cornell Medicine, New York, NY 10065, USA

[2]IDG/McGovern Institute for Brain Research, Peking University, Beijing 100871, China

[3]These authors contributed equally

[4]Lead contact

## SUMMARY

Inflammation is closely associated with many neurodegenerative disorders. Yet, whether inflammation causes, exacerbates, or responds to neurodegeneration has been challenging to define because the two processes are so closely linked. Here, we disentangle inflammation from the axon damage it causes by individually blocking cytotoxic T cell function and axon degeneration. We model inflammatory damage in mouse skin, a barrier tissue that, despite frequent inflammation, must maintain proper functioning of a dense array of axon terminals. We show that sympathetic axons modulate skin inflammation through release of norepinephrine, which suppresses activation of γδ T cells via the β2 adrenergic receptor. Strong inflammatory stimulation—modeled by application of the Toll-like receptor 7 agonist imiquimod—causes progressive γδ T cell-mediated, Sarm1-dependent loss of these immunosuppressive sympathetic axons. This removes a physiological brake on T cells, initiating a positive feedback loop of enhanced inflammation and further axon damage.

## Graphical abstract

*Correspondence: djs4002@med.cornell.edu.
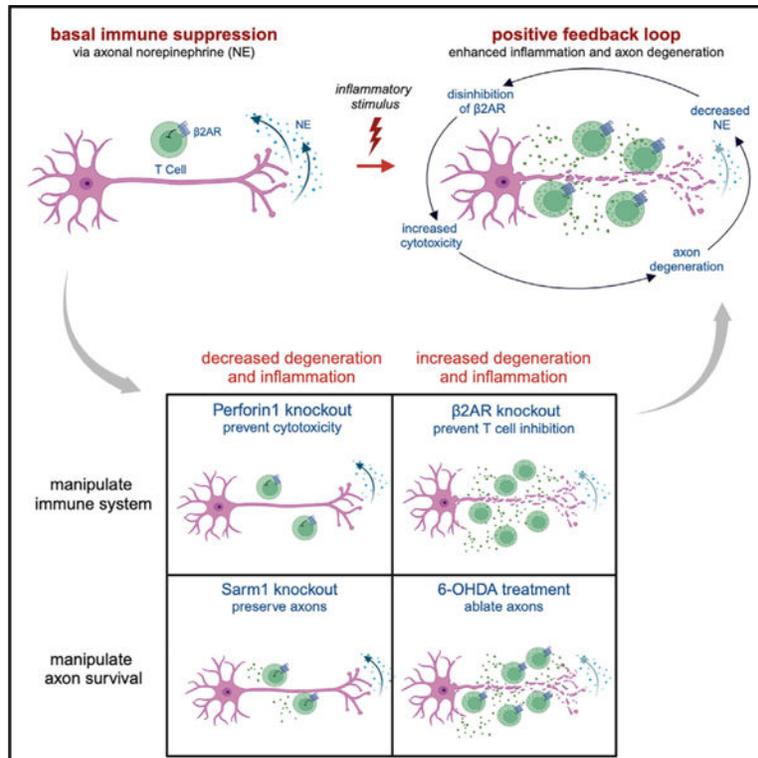
## In brief

Liu et al. study the neuronal contribution to inflammatory neurodegeneration. They develop a model in skin, allowing independent manipulation of the inflammatory response and the survival of axons. Using this model, they define a positive feedback loop that governs the relationship between inflammation and axon degeneration.

## INTRODUCTION

As a barrier tissue, the skin serves two parallel and potentially conflicting roles. The first is to enable precise sensation and thermoregulation through the careful housing of sensory and sympathetic axon terminals, while the second is to protect the body from pathogens and physical injury. In this latter capacity, skin is a site of frequent inflammation mediated by innate and adaptive immune responses.[1] While inflammation is often protective, excessive inflammation can damage tissues, including axons of the peripheral nervous system. Peripheral axons are particularly vulnerable to inflammatory damage because they lack many of the key immune-protective mechanisms present in the central nervous system, most notably a defined barrier from the blood supply.[2–4] Controlling the onset and magnitude of inflammation is therefore critical to the survival and function of barrier-innervating axons and to neuronal survival in inflamed tissues more broadly.

Our understanding of the mechanisms that protect barrier axons from inflammatory damage and how these protections are overcome is limited. Indeed, whether inflammation initiates, amplifies, or is caused by neuronal loss has been the subject of extensive debate in multiple

systems, in part because neuronal damage caused by inflammation obscures whether and how neurons contribute to inflammation.[5] Are healthy neurons passively damaged by inflammatory mediators such as T cells, or do neurons actively recruit or repel these mediators? To disentangle these roles, we used a well-defined stimulus, the Toll-like receptor 7 agonist imiquimod (IMQ), that activates a localized inflammatory response in mouse skin characterized by the appearance of interleukin-17 (IL-17)-producing γδ T cells. When applied to mouse dorsal skin, IMQ caused both progressive inflammation and marked axon loss. We used these hallmarks as a basis to test a panel of genetic and pharmacological manipulations that either block the cytotoxic function of activated T cells or enhance or inhibit the resultant axon degeneration. Together, these tools allowed us to study each aspect of T cell-axon signaling in isolation to define the signaling relationship between inflammation and axon loss in skin.

We show that inflammatory axon damage in mouse skin is controlled by a positive feedback loop between tyrosine hydroxylase (TH)-positive (TH$^+$) sympathetic axons and cytotoxic γδ T cells. In healthy skin, sympathetic axons release norepinephrine (NE), which activates β2 adrenergic receptors (β2ARs) on γδ T cells to inhibit their activation and their expression of inflammatory cytokines. Yet, once activated by IMQ, γδ T cells become cytotoxic toward sympathetic axons, driving their Sarm1-dependent degeneration, thus removing a key immunosuppressive axis. The net effect is an amplification of overall inflammation and an exacerbation of axon degeneration. Identification of this feedforward inflammatory loop and the critical modulatory role of β2AR signaling has implications for the many neurodegenerative disorders accompanied by pronounced and progressive inflammation.

## RESULTS

### Modeling inflammatory axon degeneration

Application of IMQ to mouse skin is widely used as a method to induce inflammation and to model the inflammatory skin disorder psoriasis.[6] We treated the dorsal skin of immunocompetent C57BL6/J mice with IMQ daily for six consecutive days, which, consistent with previous studies, led to progressive inflammation, plaque-like psoriasis, and tissue pathology, assessed by skin erythema, thickness, and scaling (Figures 1A and S1A−S1C).[7,8] In this context, we examined whether IMQ-dependent inflammation affected skin innervation. Here, we developed a skin preparation to visualize innervation over a large scale using whole-mount immunolabeling, tissue clearing, and light-sheet microscopy. We observed a dense reticulate structure of axons using the pan-neuronal marker PGP9.5 and a more ordered, brush-like distribution of the subset of axons immunoreactive for TH (Figure 1B). The difference in these staining patterns likely reflects the brightness of large PGP9.5$^+$ axon bundles that obscures the dimmer TH$^+$ brush-like structures. Importantly, treatment with IMQ caused a progressive decline in axon number by both markers, confirming our ability to induce inflammatory axon loss with spatial and temporal precision (Figures 1B and 1C).

In the dorsal hairy skin, expression of TH defines axons of postganglionic sympathetic neurons associated with the arrector pili muscle and sebaceous gland.[9] TH is also expressed by a subset of sensory neurons, the C-type low-threshold mechanoreceptors

(C-LTMRs); however, the brush-like structures seen in our whole-mount skin labeling are ~200 μm in length, far longer and structurally distinct from the ~20-μm-long basket-like lanceolate endings characteristic of C-LTMRs.[10] Further, treatment with 6-hydroxydopamine (6-OHDA), a catecholaminergic neurotoxin that depletes sympathetic, but not sensory, neurons—which lack the requisite dopamine transporter[11,12]—eliminated all anti-TH immunoreactive axons (Figures 4A and 4B). Thus, we conclude that the TH⁺ axons we visualize and manipulate in hairy skin are predominately sympathetic while noting that TH-negative (TH⁻) axons may also be impacted by IMQ treatment.

## γδ T cells mediate axon pathology

We next investigated the mechanism of this IMQ-induced loss with a focus on TH⁺ axons. To test whether T lymphocytes drive axon loss, we repeated IMQ treatment in *Tcrbd* mice, which lack the α, β, and γδ T cell receptors (TCRs) and are therefore deficient in the two prominent classes of tissue-damaging T cells that function in skin, α/β T cells (α and β TCRs) and γδ T cells (γ and δ TCRs)[13,14] (Figure S2). We found that knockout mice had significantly less axon (Figures 2A and 2B) and skin pathology (Figures 2C–2E) when challenged with IMQ, consistent with a lack of T cell-mediated axon damage. Which class of T cells mediates this inflammatory axon damage? Prior studies using IMQ to model psoriasis have highlighted the centrality of γδ T cells, recruited from thymic or extrathymic sources, in mediating tissue damage.[15,16] Consistent with these studies, we observed an increase in γδ T lymphocytes upon IMQ treatment using a γ-TCR GFP mouse reporter line that specifically labels γδ T cells[17] (Figures 2F and 2G) and a corresponding increase in mRNA levels of cytokines IL-17A and IL-17F, activation markers of a subset of γδ T cells (Figure 2H). Moreover, injection of an anti-γδ TCR function-blocking antibody, which depleted γδ T cells from the skin (Figures S2C and S2D), strongly reduced IMQ-induced skin pathology (Figures S2E–S2G) and, importantly, axon loss (Figures 2I and 2J).

In addition to γδ T cells, we also observed γδ TCR⁻, CD3⁺ (pan T cell marker) cells in our skin stainings (Figure S2A), likely representative of αβ T cells. A major αβ TCR⁺ population of T cells in skin expresses the marker CD8.[19] Depletion of these cells with an anti-CD8α function-blocking antibody, confirmed by reduction of CD8⁺ cells in spleen where they are abundant (Figures S3A and S3B), did not mitigate IMQ-induced skin pathology, nor axon loss (Figures S3C–S3G). From these data, we conclude that γδ TCR⁺ T cells, but CD8⁺ T cells, are the predominant axon-damaging lymphocyte population in our model. However, we do not discount that contexts exist where CD8⁺ αβ T cells can also damage axons. Indeed, CD8⁺ T cells have been implicated in loss of TH⁺ dopaminergic neurons in Parkinson's disease.[20]

How do γδ T cells damage axons? A prominent mode of T lymphocyte toxicity involves formation of cytotoxic pores in target cell plasma membranes through which granzymes and other cytotoxic molecules enter and trigger cell death.[21] Perforins are the major pore-forming proteins found in cytotoxic T lymphocytes, γδ T cells, and natural killer cells.[22,23] Indeed, we purified control and IMQ-activated γδ T cells and detected expression of Perforin-1 and IL-17A and -F (Figures S4A and S4B). Deletion of Perforin-1 in *Prf1*-knockout mice[24] did not affect basal TH⁺ axon number (Figures S4C and S4D) but did

mitigate IMQ-mediated axon loss (Figures 3A and 3B), psoriasis (Figure 3C), and skin pathology (Figures 3D and 3E). Together with the function-blocking antibody experiments (Figures 2I and 2J), these results indicate that IMQ-mediated TH[+] axon loss is driven by Perforin-1-mediated cytotoxicity by γδ T lymphocytes. We note that peripheral axons are also responsive to IL-17A,[25] which is produced by γδ T cells, which could conceivably modulate the extent of Perforin-mediated axon loss.

### Axon degeneration promotes skin inflammation

Surprisingly, overall T cell number was lower in IMQ treated Perforin-1 knockouts (Figures 3F and 3G), contrary to our expectation that the protective phenotype of these knockouts would exclusively relate to cytotoxicity, not the degree of inflammation. Moreover, the reduction of both total T cells and the γδ T cell subset was specific to the dermal skin layer (Figures 3H–3K), consistent with the exclusive projection of TH[+] axons to the dermis, not the epidermis.[26] These data drove us to consider whether IMQ-mediated axon loss itself might affect the inflammatory response. To test this hypothesis, we depleted TH[+] axons in skin through subcutaneous administration of the neurotoxic dopamine derivative 6-OHDA and confirmed their elimination via immunostaining (Figures 4A and 4B). We observed that pretreatment with 6-OHDA enhanced IMQ-induced expression of IL-17A and -F at the mRNA (Figure 4C) and protein (Figure S5B) levels and exacerbated tissue pathology (Figures 4D–4F). Importantly, depletion of TH[+] axons with 6-OHDA enhanced IMQ-mediated γδ T lymphocyte influx in skin (Figure 4G), while 6-OHDA treatment in the absence of IMQ did not affect any of these parameters.

### Preserving axons diminishes overall inflammation

Depletion of TH[+] axons enhancing IMQ-mediated inflammation suggested that these axons are immunosuppressive in dorsal skin. Sarm1 is an NAD^{+} hydrolyzing enzyme[27] that governs a pro-degenerative pathway in axons,[28] and its loss protects axons from degeneration in many contexts, including downstream of inflammatory cytokines.[29,30] We therefore reasoned that *Sarm1* deletion would allow us to study skin inflammation in the absence of the axon damage that it normally causes. Indeed, we found that IMQ-mediated axon loss was decreased in *Sarm1*-knockout mice and that this corresponded to a significant reduction in γδ T cell number and IL-17A and -F expression in skin, as well as diminished psoriasis-like tissue pathology (Figure S6). While the precise mechanism linking Perforin-1-mediated rupture of the axonal plasma membrane to activation of Sarm1-mediated axon degeneration is unknown, our results nevertheless suggest that *Sarm1* knockout is a powerful tool to block IMQ-mediated axon loss.

Sarm1 is highly expressed in neurons; however, its expression has been noted in other tissues, including immune cells.[31,32] To specifically delete Sarm1 in TH^{+} neurons, we crossed a *Sarm1* conditional knockout allele[30] to TH-Cre mice (*Th-Cre; Sarm1^{fl/fl}*). Similar to germline *Sarm1*-knockout mice, TH[+] axon density was higher following IMQ treatment in *Th-Cre; Sarm1^{fl/fl}* skin (Figures 5A and 5B). Neuronal deletion of Sarm1 similarly lessened the degree of psoriasis (Figure 5C), tissue pathology (Figures 5D and 5E), and IMQ-induced IL-17A and -F elevation (Figure 5F). Notably, protection against psoriasis-like pathology was greater in these mice compared to germline *Sarm1^{−/−}* mice (Figure S6H).

Together, these data demonstrate that TH[+] axons are immunosuppressive and that their degeneration enhances skin inflammation.

### An NE-β2AR axis

How do TH[+] axons normally suppress skin inflammation? NE is the main neurotransmitter released by TH[+] sympathetic nerve terminals, and it can have either immunosuppressive or immunostimulatory roles, depending on the cellular context.[33] While sympathetic axons can also release bioactive neuropeptides,[34] we focused our studies on NE due to its prominence as an immunosuppressive factor. Primary γδ T cells were purified by flow cytometry from subcutaneous lymph nodes after IMQ dosing and treated *in vitro* with NE, which inhibited expression of activation markers IL-17A and -F (Figure 6A). Subsequent quantification of mRNA expression of all adrenergic receptors in these acutely isolated γδ T cells identified the β2AR (Adrb2) as most abundantly expressed in these cells (Figure 6B). Consistent with this expression pattern, treatment of primary γδ T cells with β2AR agonists formoterol or clenbuterol each down-regulated IL-17A and -F expression (Figures 6C and 6D). These data are consistent with axon-derived NE signaling through β2ARs on γδ T cells to suppress inflammation in dorsal skin.

That β2AR-agonism-dampened γδ T cell activation suggested that inhibition of this immunosuppressive pathway would heighten inflammation. Indeed, a major clinical side effect of β2AR antagonists is psoriasis.[35] We therefore examined skin immune responses induced by IMQ in germline *Adrb2*-knockout mice. Notably, loss of β2AR signaling significantly exacerbated TH[+] axon loss (Figures 6E and 6F) and expression of IL-17A and -F (Figure 6G), as well as overall inflammation and psoriasis-like pathology (Figures 6H–6J), similar to TH[+] axon depletion using 6-OHDA treatment (Figure 4).

To determine the locus of β2AR action, we generated bone marrow chimeric mice by transplanting bone marrow of *Adrb2* wild-type or knockout mice into wild-type mice whose own bone marrow had been eliminated by irradiation (Figure 7A). Mice lacking Adrb2 in the bone marrow compartment (where γδ T cells originate) phenocopied germline *Adrb2*-knockout mice with respect to axon loss (Figures 7B and 7C), IL-17A and -F induction (Figure 7D), and psoriasis-like skin pathology (Figures 7E–7G). While the bone marrow niche produces immune cells in addition to γδ T cells, this result nevertheless suggests that Adrb2 functions in the immune system rather than in neurons. Together, our data support the existence of a feedforward neuroimmune loop in mouse dorsal skin. Normally, NE released by TH[+] axons inhibits skin inflammation via the β2AR on γδ T cells. Cytotoxic damage to these same axons drives their Sarm1-dependent degeneration and diminishes their immunosuppressive capacity, ultimately enhancing both inflammation and axon degeneration.

## DISCUSSION

Precise control of immune responses is critical to the proper function of barrier tissues and to nervous system function more broadly. Here, we focused on the role of TH[+] sympathetic axons in the skin as modulators of inflammation; however, inflammation occurs throughout the nervous system and affects diverse neuronal and nonneuronal cell types. There are also

many triggers of inflammation, both physiological and foreign, involving extensive interplay between multiple cell types. Together these complexities have hindered our ability to model inflammatory damage in the nervous system and to dissect its underlying mechanisms.

We use a simplified system to trigger acute inflammation and cause axon damage. IMQ is well characterized to activate resident IL-17-expressing γδ T cells in skin, resulting in tissue damage that is used as a preclinical model of psoriasis.[6] We reasoned that application of IMQ would enable precise control over the timing, location, and cellular composition of inflammation, a controlled setting to study inflammatory axon degeneration. Indeed, we find that application of IMQ to mouse dorsal skin causes progressive, γδ T cell-dependent axon degeneration. In the context of this model, we identify a neurodegenerative positive feedback loop that reinforces inflammatory damage. Blocking IMQ-mediated axon damage by either impairing the cytotoxic function of activated T cells or removing an axon-intrinsic pro-degenerative pathway in TH$^+$ axons lessens overall inflammation. Further, ablation of TH$^+$ axons or removal of Adrb2 in immune cells—the receptor for TH$^+$ axon-derived NE—enhances IMQ-mediated skin inflammation. Together, these data argue that TH$^+$ sympathetic axons normally suppress skin inflammation and that their degeneration enhances inflammation.

Dying cells release immune-stimulatory molecules that promote the clearance of cellular debris and the maintenance of tissue homeostasis.[36] While we do not rule out the importance of these signals in exacerbating IMQ-mediated axon loss, we note that axon depletion through 6-OHDA in the absence of IMQ does not stimulate a detectable immune response (Figures 4C–4E). Instead, our data argue that loss of an immunosuppressive β2AR signaling axis, resulting from T cell-induced degeneration of TH$^+$ axons, underlies the cycle of inflammatory axon damage that we describe. We show that NE, a neuromodulator known to be released from TH$^+$ axons, suppresses γδ T cell activation. Further, deletion of its receptor, β2AR, in the immune compartment phenocopies experimental TH$^+$ axon ablation and enhances IMQ-mediated inflammation. These data are consistent with an NE-β2AR signaling axis acting as a physiological brake on skin inflammation that, when interrupted, enhances inflammation and subsequent inflammatory axon damage.

Positive feedback loops such as the one we define can predispose toward rapid and uncontrolled amplification,[37] which may account for the progressive inflammation and neuronal loss that characterize many neurodegenerative pathologies. Control over the initiation and early amplification of inflammation would therefore be critical determinants of whether these loops are engaged. Intriguingly, sensory neurons themselves can drive early immune responses through the release of pro-inflammatory chemokines[38–40] and other immune-stimulating peptides,[41] thus providing additional, complementary mechanisms to regulate the dynamics of inflammatory loops. Finally, our findings highlight the importance of counteracting positive feedback loops to resolve inflammatory responses, especially when endogenous immunosuppressive mechanisms such as regulatory T cells have been exhausted. In skin, β2AR agonism would likely dampen inflammatory responses by compensating for the loss of sympathetic axons. Elsewhere, direct engagement of inhibitory receptors on infiltrating lymphocytes or on activated CNS-resident immune cells may serve a similar role to counteract neuroinflammation in the context of neurodegenerative disorders.

### Limitations of the study

The neuroimmune feedback loop that we describe was identified in the context of IMQ stimulation as the initial source of inflammation. As such, other inflammatory stimuli may have distinct relationships with nerve-derived signals and potentially engage different immune cell populations and with distinct ligand-receptor pairs.

## STAR★METHODS

### RESOURCE AVAILABILITY

**Lead contact—**Further information and requests for resources and reagents should be directed to and will be fulfilled by the lead contact, David J. Simon (djs4002@med.cornell.edu).

**Materials availability—**This study did not generate new unique reagents.

#### Data and code availability

- All data reported in this paper will be shared by the lead contact upon request

- This paper does not report original code.

- Any additional information required to reanalyze the data reported in this work paper is available from the lead contact upon request.

### EXPERIMENTAL MODEL AND STUDY PARTICIPANT DETAILS

Experiments were performed on female mice between 8 and 10 weeks of age unless otherwise specified, and in accordance with approved protocols at Weill Cornell Medicine or Peking University. Wild type C57BL/6 mice were purchased from the Jackson Labs or Charles River International. *Trcbd* mice, an intercross of the *Tcrb* and *Tcrd* knockout lines, were purchased from Jackson Labs (Cat# 002122, RRID:IMSR_JAX:002122) and bred as homozygous double knockouts. Prf1 mice were purchased from Jackson Labs (Cat # 002407, RRID:IMSR_JAX:002407) and bred as homozygous knockouts. *Sarm1* knockout (Cat#JAX:018069, RRID:IMSR_JAX:018069) mice were purchased from Jackson Laboratory and backcrossed for one generation to wild type. Heterozygous offspring were then intercrossed to generate Sarm1 WT and KO littermates. To generate *Th-Cre;Sarm1$^{fl/fl}$* mice, *Th-Cre* (Cat#JAX:008601, RRID:IMSR_-JAX:008601) mice were purchased from the Jackson Labs and crossed to a *Sarm1$^{fl/fl}$* mouse that we previously generated.[30] *Adrb2* wild type and knockout mice were generated by backcrossing the strain *Adrb1;Adrb2* (JAX 003810, RRID:IMSR_JAX:003810) to C57BL/6 for two generations to isolate heterozygous *Adrb2* mice for intercrosses to generate WT and KO mice. Tcrd-H2B-eGFP mice were provided by Josef Anrather (Weill Cornell), originally received from Jackson Labs (Cat # 016941, RRID:IMSR_JAX: 016941). Homozygous mice were bred to C57BL/6J wild type mice to generate heterozygous GFP-expressing mice for experimentation.

### METHOD DETAILS

**Skin treatments—**Imiquimod: Female mice at 8 to 10 weeks of age received a daily topical dose of 5% Imiquimod (IMQ) cream (Aldara; 3M Pharmaceuticals) for 3 or

6 consecutive days, as indicated. On the day prior to the first treatment, mice were anesthetized and a 2cm2 region of hair on their backs was shaved with an electric razor followed and cleared of remaining hairs using a depilatory cream (Nair; Church & Dwight Co., Inc.). Subsequent IMQ treatments were performed under brief inhaled isoflurane anesthesia. We note that female mice were used because, in our experience, male mice treated with IMQ became hyper-aggressive and fought with each other, necessitating single housing across many cohorts. IMQ-induced inflammatory gene expression in C57BL6 mice is unaffected by gender.[42] 6-OHDA: Each mouse was treated with 500μg 6-OHDA (dissolved in 200 μL sterile PBS containing 0.01% ascorbic acid; Sigma-Aldrich), administered by subcutaneous injection daily for 2 days. A 2cm$^2$ patch of dorsal hair was removed under anesthesia 3 days after the last injection. Mice next received 5 daily treatments of IMQ.

**Generation of bone marrow chimeric mice**—For the establishment of bone-marrow chimeric mice (BMCM), wild-type female recipient mice at 8 weeks of age received 11 Gy of X-ray radiation across two equal doses, given 2 h apart in the Peking University animal facility, according to published protocols.[43] This treatment eliminated the bone marrow population of recipient mice. Donor bone marrow was harvested from 8 week-old female mice of the indicated genotypes as previously published.[30] In brief, femurs were harvested, flushed with RPMI-1640 media, followed by red blood cell lysis and filtration with a 75μm strainer. $2 \times 10^6$ cells of the resultant bone marrow suspension were transplanted into each irradiated mouse, 30 min post-exposure, via intravenous injection. Chimeric mice were treated with IMQ 5 weeks after the transplantation.

Validation of chimerism rate was performed as previously published.[44]

**Whole mount immunolabeling and 3D imaging**—At the conclusion of each experiment dorsal skin was harvested following perfusion with 20 mL of phosphate-buffered saline (PBS)/heparin (10 μg/mL) and 20 mL of PBS/1% paraformaldehyde (PFA)/10% sucrose/heparin (10 μg/mL). Skin was removed and fixed in PBS/0.5%PFA at 4°C overnight. Next day, the tissue was washed with PBS at room temperature for 30 min, three times. All subsequent incubation steps were performed with gentle rotating.

Whole mount immunolabeling of axons in skin was performed using the iDISCO method.[45] For detection of γδ T cells we used a modified to the iDISCO protocol where acetone replaced methanol for the initial tissue dehydration.[46] Skin samples were washed sequentially with 20%, 40%, 60%, 80% and 100% methanol (in ddH$_2$O) for 1 h at room temperature. Samples were next washed in 100% methanal for 1 h and then bleached with 5% H$_2$O$_2$ (1 volume of 30%H$_2$O$_2$ for 5 volumes of methanol, ice-cold) at 4°C overnight. After bleaching, samples were re-hydrated sequentially in 80%, 60%, 40%, 20% methanol in ddH$_2$O for 1 h at room temperature. The tissues were then washed with PBS at room temperature for 30 min, twice, followed by PBS/0.2% Triton X-100/0.1% deoxycholate/10% DMSO, overnight. The tissues were blocked with PBS/0.2% Triton X-100/10% DMSO/5% normal donkey serum at room temperature overnight and then immunolabeled with intended primary antibodies (1:500 dilution) in PBS/0.1% Tween 20/heparin (10 μg/mL)/5% normal donkey serum at room temperature for 48 h. The primary antibodies used in this study were

rabbit anti-PGP9.5 (ProteinTech Group, RRID:AB_2210497), and rabbit anti-TH (Millipore, RRID:AB_390204).The tissues were then washed with PBS/0.1% Tween 20/heparin (10 μg/mL) at room temperature for 12 h, with the fresh buffer added every 2 h. The tissues were further immunolabeled with the corresponding Alexa Fluor dye–conjugated secondary antibodies (1:500 dilution; Thermo Fisher Scientific) in PBS/0.1% Tween 20/heparin (10 μg/mL)/5% normal donkey serum at room temperature for 48 h. The tissues were washed with PBS/0.1% Tween 20/heparin (10 μg/mL) at room temperature for 24 h, with fresh buffer added every 6 h. The immunolabeled lung tissues were washed with PBS at room temperature for 2 h and embedded in PBS/1% agarose before the optical clearing. The tissue blocks were incubated at room temperature with 20% methanol (diluted in ddH2O) for 1 h three times, 40% methanol for 1 h, 60% methanol for 1 h, 80% methanol for 1 h, 100% methanol for 1 h, and 100% methanol overnight. The tissue blocks were then incubated at room temperature with the mixture of dichloromethane and methanol (2:1) for 3 h, followed by 100% dichloromethane for 30 min three times. The tissue blocks were lastly incubated at room temperature with 100% dibenzyl ether for 12 h twice.

For acetone-based iDISCO, skin tissues were treated at room temperature with 25% acetone (diluted in ddH2O) for 1 h, 50% acetone for 3 h, and 25% acetone for 1 h. The tissues were washed with PBS at room temperature for 30 min twice, followed by PBS/30% sucrose for 2 h. The tissues were bleached in PBS/30% sucrose/1%$H_2O_2$ at 4°C overnight. The tissues were then washed with PBS at room temperature for 30 min twice, followed by PBS/ 0.2% Triton X-100/0.1% deoxycholate/10% DMSO overnight. The tissues were blocked, incubated with primary and secondary antibodies, embedding, and cleared as described in iDISCO. The primary antibodies used were Armenian hamster anti-γδ TCR (Biolegend, RRID:AB_313830) and rabbit anti-TH (Millipore, RRID:AB_390204).

**PASI scoring—**Skin inflammation resulting from IMQ treatment was evaluated by three indexes: erythema, thickness, and scale, based on an established methodology.[8] Briefly, each of these pathologies was scored from 0 to 4 (0: none, 1: mild, 2: moderate, 3: marked, 4: severe). The reported psoriasis area severity index (PASI) score is the sum of these three values.

**Histology—**For histologic examination, skin was dissected after perfusion, postfixed with 4% PFA at 4°C overnight, and processed for hematoxylin and eosin (H&E) staining. Briefly, skin was embedded in paraffin, sectioned, stained with H&E to illustrate the nuclear and cytoplasmic architecture of each section. Scoring of IMQ-treated skin tissues was performed following the established Baker's standard.[18] Analysis was performed on 5 randomly selected regions (×20 magnification) from sections of each tissue.

**Quantification of mRNA expression—**Expression of genes of interest was measured using Real-Time Quantitative PCR (qPCR). For analysis of skin, dorsal skin was acutely removed and homogenized in TRIzol (Thermo Fisher Scientific) by a rotor-stator homogenizer. Total RNA was subsequently isolated, reverse transcribed by PrimeScript RT reagent Kit (Takara) and quantified using SYBR Green Real-Time PCR Kit (Thermo Fisher Scientific).

**FACS analysis**—To quantify immune cell numbers in dorsal skin, a 1cm² skin punch biopsy was performed, removed of subcutaneous adipose tissue, and incubated in RPMI-1640 (Sigma-Aldrich) containing Dispase II (Sigma-Aldrich), Golgi-Plug (1:1000, BD Biosciences), 2% FBS (Gibco), 1% HEPES (Corning, pH = 7.2–7.6), 1%Penicillin/ streptomycin (Corning) at 37°C for 30 min. Next, the dermis was separated from the epidermis and finely minced into small pieces with scissors, digested in RPMI-1640 with 1 mg/mL Collagenase IV (Sigma-Aldrich), Golgi Plug (1:1000), 0.5 mg/mL Hyaluronidase (Sigma-Aldrich), 100ug/mL DNaseI (Sigma-Aldrich) at 37°C for 30 min and passed through a 70-μm cell strainer. This resulted in a single cell suspension. Cells were then stimulated with 75 ng/mL phorbol 12-myristate 13-acetate/ionomycin (Santa Cruz) for 4 h in the presence of GolgiPlug (1:1000), then pre-incubated with Fc Block (eBioscience) and stained with surface markers – CD45 (RRID: AB_312979) CD3(RRID: AB_10900227), γδ TCR (RRID: AB_313830) – and intracellular marker IL17A (RRID: AB_763580) successively. Samples were analyzed using a BD LSRFortessa (BD Biosciences). FACS data were analyzed by FlowJo (https://www.flowjo.com).

***In vitro* treatment**—Skin subcutaneous lymph nodes were homogenized manually through 70-μm cell strainers. Cells were stained with antibodies to CD45 (Biolegend, RRID: AB_312979), CD3 (Biolegend, RRID:AB_312663) and γδ TCR (Biolegend, RRID:AB_313830), and sorted using a BD FACSAria (BD Biosciences). Primary γδ T cells [CD45⁺CD3+γδ TCR+] were suspended in RPMI-1640 containing 10% heat-inpenicilli/ penicillin (100 U/ml)/streptomycin (100 μg/mL) and incubated at 37°C for 2hrs. Cells were subsequently treated with 20 μmol/L of either norepinephrine (Sigma), Formoterol (Sigma), or Clenbuterol (Sigma). Total RNA was then extracted using the RNeasy Mini Kit (Qiagen) and analyzed by qPCR as above.

**Immune cell quantification by immunofluorescence**—To quantity T cell number in immunostained tissue sections, we used the CellCounter plugin in ImageJ (https:// imagej.net/ij/plugins/cell-counter.html) which allows for manual cell detection. To quantify the number of γδ T cells in wholemount immunostaining, the Cell function in Imaris (version 10.0.0) was used, with detection parameters set at 5μm in the X axis and 70 μm in the z axis, which accounts for the frequent z axis distortion seen using light sheet microscopy. Parameters were manually adjusted by examining labeling accuracy of cells in representative X-Y optical slices. To count T cell number in tissue sections from spleen, we used Ilastik (www.ilastik.org), using the Cell Density counting workflow. A model was trained on two manually annotated images from both the control and experimental groups. The model then outputted the estimated cell counts for each image.

**Axon quantification**—Axon number in each sample is measured from a maximal z axis projection of each whole mount immunolabeled skin sample, performed using Imaris software. This reflects a manual measurement of the total length of immunolabeled axon segments in the dermal and/or epidermal regions of skin. The large subdermal branches visible in PGP9.5 and TH stains are not quantified.

**Bulk RNA sequencing of gamma delta T cells**—RNA sequencing of FACS-purified γδ T cells was performed by pooling inguinal lymph nodes from one control and one IMQ-treated mouse. For IMQ treatment the mouse was shaved and treated with depilation cream near the groin with $1.5 \times 1.5$ cm application of 5% IMQ cream (Aldara) applied daily for 6 consecutive days. Freshly collected inguinal lymph nodes were mashed through 70-μm cell strainers. The cells were stained with FACS antibodies and sorted as CD45+ (Biolegend, RRID: AB_312979), CD3+ (Biolegend, RRID:AB_312663), γδ TCR+ (Biolegend, RRID:AB_313830) live cells (Figure S4A) on a BD FACSAria Fusion. Total RNA was harvested using phenol/chloroform, followed by mRNA isolation. cDNA synthesis, end repair, adaptor ligation and PCR were conducted sequentially (COMPANY) to prepare mRNA libraries. The obtained libraries were sequenced on MGISEQ-2000 system. The sequencing data was filtered with SOAPnuke (v1.5.2), mapped to the assembled unique genes using Bowtie2 (v2.2.5), and the expression level of genes was calculated by RSEM (v1.3.1). Total normalize reads for each gene are presented (Figure S4B).

## ELISA

To assess cytokine protein abundance, collected skin tissue was homogenized in cold PBS and centrifuged at 10,000 g for 15 min to obtain supernatant for detection by ELISA (Meimian, Jiangsu, China; catalog no. MM-0759M1 (IL-17A); MM-1129M1 (IL-17F)) according to the manufacturer's instructions.

**Function blocking antibody treatment**—For CD8 and γδ T cell depletion, 500 μg of either anti-CD8a (clone: 53–6.7, Bio X Cell, catalog no. BE0004–1) or anti-TCR γδ (clone: UC7–13D5, Bio X Cell, catalog no. BE0070) antibodies were injected intraperitoneally, one day prior to IMQ treatment and 3 days after the first treatment with IMQ. As a negative control to CD8 and γδ TCR depletion, control cohorts received intraperitoneal injection of 500 μg of InVivoPlus rat immunoglobulin G2a (IgG2a) isotype control (clone 2A3, Bio X Cell, catalog no. BE0089) and InVivoMAb polyclonal Armenian hamster IgG (Bio X Cell, catalog no. BE0091), respectively.

## QUANTIFICATION AND STATISTICAL ANALYSIS

Statistical analysis was performed using GraphPad Prism v.8. Experimenters were not blinded to treatment condition because IMQ treated mice are easily distinguishable based on redness of their skin, and IMQ treated skin samples (whole mount immunolabeled or tissue sections) are easily distinguished based on the thickness of their skin, as has been previously described.[6]

## Supplementary Material

Refer to Web version on PubMed Central for supplementary material.

# REFERENCES

1. Pasparakis M, Haase I, and Nestle FO (2014). Mechanisms regulating skin immunity and inflammation. Nat. Rev. Immunol. 14, 289–301. 10.1038/nri3646. [PubMed: 24722477]

2. Croese T, Castellani G, and Schwartz M (2021). Immune cell compartmentalization for brain surveillance and protection. Nat. Immunol. 22, 1083–1092. 10.1038/s41590-021-00994-2. [PubMed: 34429552]

3. Chiu IM, von Hehn CA, and Woolf CJ (2012). Neurogenic inflammation and the peripheral nervous system in host defense and immunopathology. Nat. Neurosci. 15, 1063–1067. 10.1038/nn.3144. [PubMed: 22837035]

4. Ren K, and Dubner R (2010). Interactions between the immune and nervous systems in pain. Nat. Med. 16, 1267–1276. 10.1038/nm.2234. [PubMed: 20948535]

5. Martini R, and Willison H (2016). Neuroinflammation in the peripheral nerve: Cause, modulator, or bystander in peripheral neuropathies? Glia 64, 475–486. 10.1002/glia.22899. [PubMed: 26250643]

6. Flutter B, and Nestle FO (2013). TLRs to cytokines: mechanistic insights from the imiquimod mouse model of psoriasis. Eur. J. Immunol. 43, 3138–3146. 10.1002/eji.201343801. [PubMed: 24254490]

7. van der Fits L, Mourits S, Voerman JSA, Kant M, Boon L, Laman JD, Cornelissen F, Mus AM, Florencia E, Prens EP, and Lubberts E (2009). Imiquimod-induced psoriasis-like skin inflammation in mice is mediated via the IL-23/IL-17 axis. J. Immunol. 182, 5836–5845. 10.4049/jimmunol.0802999. [PubMed: 19380832]

8. Wu DH, Zhang MM, Li N, Li X, Cai QW, Yu WL, Liu LP, Zhu W, and Lu CJ (2019). PSORI-CM02 alleviates IMQ-induced mouse dermatitis via differentially regulating pro- and anti-inflammatory cytokines targeting of Th2 specific transcript factor GATA3. Biomed. Pharmacother. 110, 265–274. 10.1016/j.biopha.2018.11.092. [PubMed: 30513504]

9. Glatte P, Buchmann SJ, Hijazi MM, Illigens BMW, and Siepmann T (2019). Architecture of the Cutaneous Autonomic Nervous System. Front. Neurol. 10, 970. 10.3389/fneur.2019.00970. [PubMed: 31551921]

10. Li L, Rutlin M, Abraira VE, Cassidy C, Kus L, Gong S, Jankowski MP, Luo W, Heintz N, Koerber HR, et al. (2011). The functional organization of cutaneous low-threshold mechanosensory neurons. Cell 147, 1615–1627. 10.1016/j.cell.2011.11.027. [PubMed: 22196735]

11. Glinka Y, Gassen M, and Youdim MB (1997). Mechanism of 6-hydroxydopamine neurotoxicity. J. Neural. Transm. Suppl. 50, 55–66. 10.1007/978-3-7091-6842-4_7. [PubMed: 9120425]

12. Sharma N, Flaherty K, Lezgiyeva K, Wagner DE, Klein AM, and Ginty DD (2020). The emergence of transcriptional identity in somatosensory neurons. Nature 577, 392–398. 10.1038/s41586-019-1900-1. [PubMed: 31915380]

13. Mombaerts P, Clarke AR, Hooper ML, and Tonegawa S (1991). Creation of a large genomic deletion at the T-cell antigen receptor beta-subunit locus in mouse embryonic stem cells by gene targeting. Proc. Natl. Acad. Sci. USA 88, 3084–3087. 10.1073/pnas.88.8.3084. [PubMed: 1826563]

14. Itohara S, Mombaerts P, Lafaille J, Iacomini J, Nelson A, Clarke AR, Hooper ML, Farr A, and Tonegawa S (1993). T cell receptor delta gene mutant mice: independent generation of alpha beta T cells and programmed rearrangements of gamma delta TCR genes. Cell 72, 337–348. 10.1016/0092-8674(93)90112-4. [PubMed: 8381716]

15. Tortola L, Rosenwald E, Abel B, Blumberg H, Schäfer M, Coyle AJ, Renauld JC, Werner S, Kisielow J, and Kopf M (2012). Psoriasiform dermatitis is driven by IL-36-mediated DC-keratinocyte crosstalk. J. Clin. Invest. 122, 3965–3976. 10.1172/JCI63451. [PubMed: 23064362]

16. Okura I, Kamata M, Asano Y, Mitsui A, Shimizu T, Sato S, and Tada Y (2021). Fingolimod ameliorates imiquimod-induced psoriasiform dermatitis by sequestering interleukin-17-producing ?d T cells in secondary lymph nodes. J. Dermatol. Sci. 102, 116–125. 10.1016/j.jdermsci.2021.04.004. [PubMed: 33888401]

17. Prinz I, Sansoni A, Kissenpfennig A, Ardouin L, Malissen M, and Malissen B (2006). Visualization of the earliest steps of gammadelta T cell development in the adult thymus. Nat. Immunol. 7, 995–1003. 10.1038/ni1371. [PubMed: 16878135]

18. Luo DQ, Wu HH, Zhao YK, Liu JH, and Wang F (2016). Original Research: Different imiquimod creams resulting in differential effects for imiquimod-induced psoriatic mouse models. Exp. Biol. Med. 241, 1733–1738. 10.1177/1535370216647183.

19. Kao YS, Mamareli P, Dhillon-LaBrooy A, Stüve P, Godoy GJ, Velasquez LN, Raker VK, Weidenthaler-Barth B, Boukhallouk F, Rampoldi F, et al. (2023). Targeting ACC1 in T cells ameliorates psoriatic skin inflammation. J. Mol. Med. 101, 1153–1166. 10.1007/s00109-023-02349-w. [PubMed: 37594540]

20. Weiss F, Labrador-Garrido A, Dzamko N, and Halliday G (2022). Immune responses in the Parkinson's disease brain. Neurobiol. Dis. 168, 105700. 10.1016/j.nbd.2022.105700. [PubMed: 35314321]

21. Russell JH, and Ley TJ (2002). Lymphocyte-mediated cytotoxicity. Annu. Rev. Immunol. 20, 323–370. 10.1146/annurev.immunol.20.100201.131730. [PubMed: 11861606]

22. Voskoboinik I, Whisstock JC, and Trapani JA (2015). Perforin and granzymes: function, dysfunction and human pathology. Nat. Rev. Immunol. 15, 388–400. 10.1038/nri3839. [PubMed: 25998963]

23. O'Neill K, Pastar I, Tomic-Canic M, and Strbo N (2020). Perforins Expression by Cutaneous Gamma Delta T Cells. Front. Immunol. 11, 1839. 10.3389/fimmu.2020.01839. [PubMed: 32922397]

24. Kägi D, Ledermann B, Bürki K, Seiler P, Odermatt B, Olsen KJ, Podack ER, Zinkernagel RM, and Hengartner H (1994). Cytotoxicity mediated by T cells and natural killer cells is greatly impaired in perforin-deficient mice. Nature 369, 31–37. 10.1038/369031a0. [PubMed: 8164737]

25. Enamorado M, Kulalert W, Han SJ, Rao I, Delaleu J, Link VM, Yong D, Smelkinson M, Gil L, Nakajima S, et al. (2023). Immunity to the microbiota promotes sensory neuron regeneration. Cell 186, 607–620.e17. 10.1016/j.cell.2022.12.037. [PubMed: 36640762]

26. Roosterman D, Goerge T, Schneider SW, Bunnett NW, and Steinhoff M (2006). Neuronal control of skin function: the skin as a neuroimmunoendocrine organ. Physiol. Rev. 86, 1309–1379. 10.1152/physrev.00026.2005. [PubMed: 17015491]

27. Essuman K, Summers DW, Sasaki Y, Mao X, DiAntonio A, and Milbrandt J (2017). The SARM1 Toll/Interleukin-1 Receptor Domain Possesses Intrinsic NAD(+) Cleavage Activity that Promotes Pathological Axonal Degeneration. Neuron 93, 1334–1343.e5. 10.1016/j.neuron.2017.02.022. [PubMed: 28334607]

28. Sambashivan S, and Freeman MR (2021). SARM1 signaling mechanisms in the injured nervous system. Curr. Opin. Neurobiol. 69, 247–255. 10.1016/j.conb.2021.05.004. [PubMed: 34175654]

29. Ko KW, Milbrandt J, and DiAntonio A (2020). SARM1 acts downstream of neuroinflammatory and necroptotic signaling to induce axon degeneration. J. Cell Biol. 219, e201912047. 10.1083/jcb.201912047. [PubMed: 32609299]

30. Sun Y, Wang Q, Wang Y, Ren W, Cao Y, Li J, Zhou X, Fu W, and Yang J (2021). Sarm1-mediated neurodegeneration within the enteric nervous system protects against local inflammation of the colon. Protein Cell 12, 621–638. 10.1007/s13238-021-00835-w. [PubMed: 33871822]

31. Jin L, Zhang J, Hua X, Xu X, Li J, Wang J, Wang M, Liu H, Qiu H, Chen M, et al. (2022). Astrocytic SARM1 promotes neuroinflammation and axonal demyelination in experimental autoimmune encephalomyelitis through inhibiting GDNF signaling. Cell Death Dis. 13, 759. 10.1038/s41419-022-05202-z. [PubMed: 36055989]

32. Panneerselvam P, Singh LP, Selvarajan V, Chng WJ, Ng SB, Tan NS, Ho B, Chen J, and Ding JL (2013). T-cell death following immune activation is mediated by mitochondria-localized SARM. Cell Death Differ. 20, 478–489. 10.1038/cdd.2012.144. [PubMed: 23175186]

33. Gaskill PJ, and Khoshbouei H (2022). Dopamine and norepinephrine are embracing their immune side and so should we. Curr. Opin. Neurobiol. 77, 102626. 10.1016/j.conb.2022.102626. [PubMed: 36058009]

34. Benarroch EE (1994). Neuropeptides in the sympathetic system: presence, plasticity, modulation, and implications. Ann. Neurol. 36, 6–13. 10.1002/ana.410360105. [PubMed: 8024263]

35. Gold MH, Holy AK, and Roenigk HH Jr. (1988). Beta-blocking drugs and psoriasis. A review of cutaneous side effects and retrospective analysis of their effects on psoriasis. J. Am. Acad. Dermatol. 19, 837–841. [PubMed: 2903871]

36. Yatim N, Cullen S, and Albert ML (2017). Dying cells actively regulate adaptive immune responses. Nat. Rev. Immunol. 17, 262–275. 10.1038/nri.2017.9. [PubMed: 28287107]

37. Ingolia NT, and Murray AW (2007). Positive-feedback loops as a flexible biological module. Curr. Biol. 17, 668–677. 10.1016/j.cub.2007.03.016. [PubMed: 17398098]

38. Wang Q, Zhang S, Liu T, Wang H, Liu K, Wang Q, and Zeng W (2018). Sarm1/Myd88–5 Regulates Neuronal Intrinsic Immune Response to Traumatic Axonal Injuries. Cell Rep. 23, 716–724. 10.1016/j.celrep.2018.03.071. [PubMed: 29669278]

39. Wlaschin JJ, Gluski JM, Nguyen E, Silberberg H, Thompson JH, Chesler AT, and Le Pichon CE (2018). Dual leucine zipper kinase is required for mechanical allodynia and microgliosis after nerve injury. Elife 7, e33910. 10.7554/eLife.33910. [PubMed: 29968565]

40. Riol-Blanco L, Ordovas-Montanes J, Perro M, Naval E, Thiriot A, Alvarez D, Paust S, Wood JN, and von Andrian UH (2014). Nociceptive sensory neurons drive interleukin-23-mediated psoriasiform skin inflammation. Nature 510, 157–161. 10.1038/nature13199. [PubMed: 24759321]

41. Klein Wolterink RGJ, Wu GS, Chiu IM, and Veiga-Fernandes H (2022). Neuroimmune Interactions in Peripheral Organs. Annu. Rev. Neurosci. 45, 339–360. 10.1146/annurev-neuro-111020-105359. [PubMed: 35363534]

42. Swindell WR, Michaels KA, Sutter AJ, Diaconu D, Fritz Y, Xing X, Sarkar MK, Liang Y, Tsoi A, Gudjonsson JE, and Ward NL (2017). Imiquimod has strain-dependent effects in mice and does not uniquely model human psoriasis. Genome Med. 9, 24. 10.1186/s13073-017-0415-3. [PubMed: 28279190]

43. Eng J, Orf J, Perez K, Sawant D, and DeVoss J (2020). Generation of bone marrow chimeras using X-ray irradiation: comparison to cesium irradiation and use in immunotherapy. J. Biol. Methods 7, e125. 10.14440/jbm.2020.314. [PubMed: 32206674]

44. Jiang H, Ding X, Cao Y, Wang H, and Zeng W (2017). Dense Intra-adipose Sympathetic Arborizations Are Essential for Cold-Induced Beiging of Mouse White Adipose Tissue. Cell Metab. 26, 686–692.e3. 10.1016/j.cmet.2017.08.016. [PubMed: 28918935]

45. Renier N, Wu Z, Simon DJ, Yang J, Ariel P, and Tessier-Lavigne M (2014). iDISCO: a simple, rapid method to immunolabel large tissue samples for volume imaging. Cell 159, 896–910. 10.1016/j.cell.2014.10.010. [PubMed: 25417164]

46. Liu T, Yang L, Han X, Ding X, Li J, and Yang J (2020). Local sympathetic innervations modulate the lung innate immune responses. Sci. Adv. 6, eaay1497. 10.1126/sciadv.aay1497. [PubMed: 32426489]

## Highlights

- Development of a skin model to study the neuronal contribution to inflammatory axon loss

- Adrenergic signaling is an axon-derived physiological brake limiting inflammation

- Initial axon loss initiates a feedback loop that enhances inflammation and axon degeneration
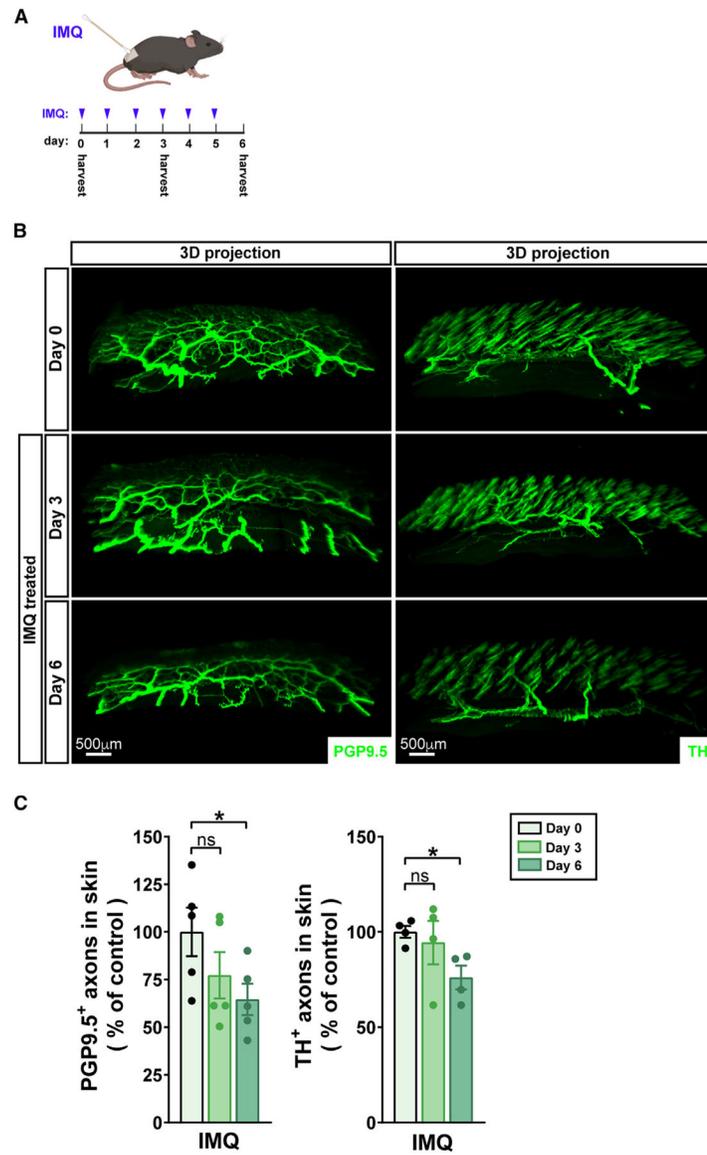
**Figure 1. A model for T cell-mediated axon loss in mouse skin**

(A) Mouse dorsal skin was treated with a non-toxic cream or 5% IMQ cream once per day for three or six consecutive days, with tissue collection as indicated.

(B) Axonal projections throughout large sections of skin were processed by whole-mount immunolabeling for PGP9.5 or TH and visualized using light-sheet microscopy. Representative 3D projections of 1-mm-thick skin samples are shown. A secondary antibody-alone staining was performed in parallel to rule out that the brush-like anti-TH immunoreactivity is due to non-specific staining of hair follicles (Figure S1D).

(C) Axon number from (B) quantified for each time point as mean ± SEM. n = 4 (TH) and 5 (PGP9.5). Here and throughout, $*p < 0.05$, $**p < 0.01$, $***p < 0.001$, and $****p < 0.0001$ (unpaired, two-tailed t test). Histological measurements of the skin response to IMQ among the samples stained for PGP9.5 are presented in Figure S1.
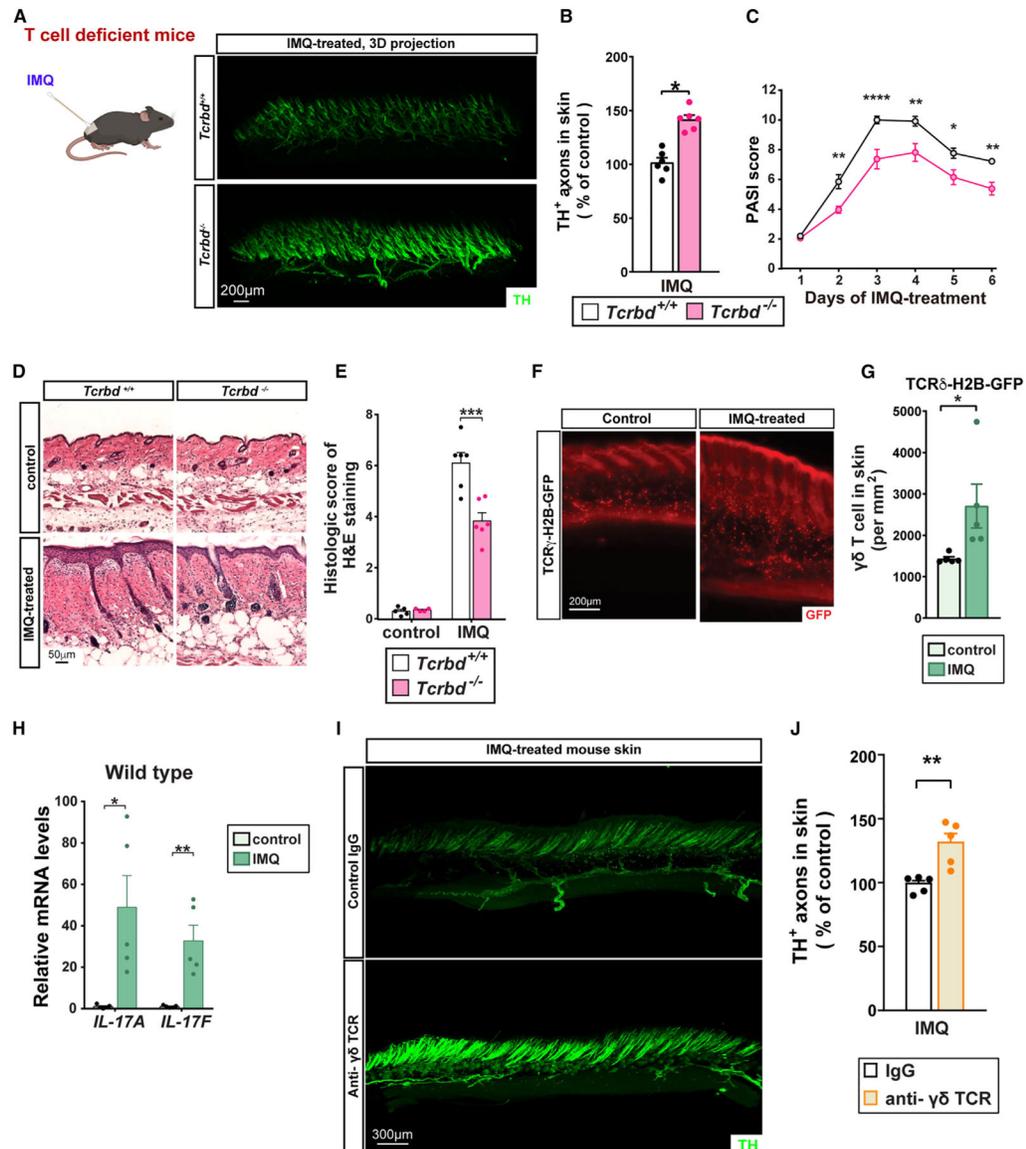
**Figure 2. γδ T cells are required for IMQ-mediated axon loss and tissue damage**

(A and B) Mice of the indicated genotypes were subjected to 6 days of daily IMQ treatment. TH$^+$ axons were visualized at the terminal time point (A), and their number was quantified in (B). n = 6, mean ± SEM, unpaired, two-tailed t test.

(C) The response to IMQ was further assayed by psoriasis area severity index (PASI). n = 6, mean ± SEM, two-way ANOVA with Sidak's correction.

(D and E) (D) IMQ-induced tissue damage was assessed by H&E and quantified in (E) using Baker's standard.[18] n = 4 (control) or 6 (IMQ), mean ± SEM, two-way ANOVA with Tukey's post hoc test.

(F) γδ T cell number was determined using a γ-TCR GFP mouse reporter line that specifically labels γδ T cells. Skin was imaged following whole-mount immunolabeling for GFP in control or after IMQ treatment (6 days). Representative images from single

optical sections shown. Cell number was manually quantified across a 2 mm$^2$ area in (G). n = 5, mean ± SEM, unpaired, two-tailed t test.

(H) Expression levels of *IL-17A* and *IL-17F* in skin samples collected 24 h after the last IMQ treatment were determined by the qPCR. n = 5, mean ± SEM, unpaired, two-tailed t test.

(I) Mice were treated with control IgG or an anti-γδ TCR function-blocking antibody, followed by IMQ treatments for 6 days. TH$^+$ axons were visualized at the terminal time point, and their number was quantified (J). n = 5, mean ± SEM, unpaired, two-tailed t test.
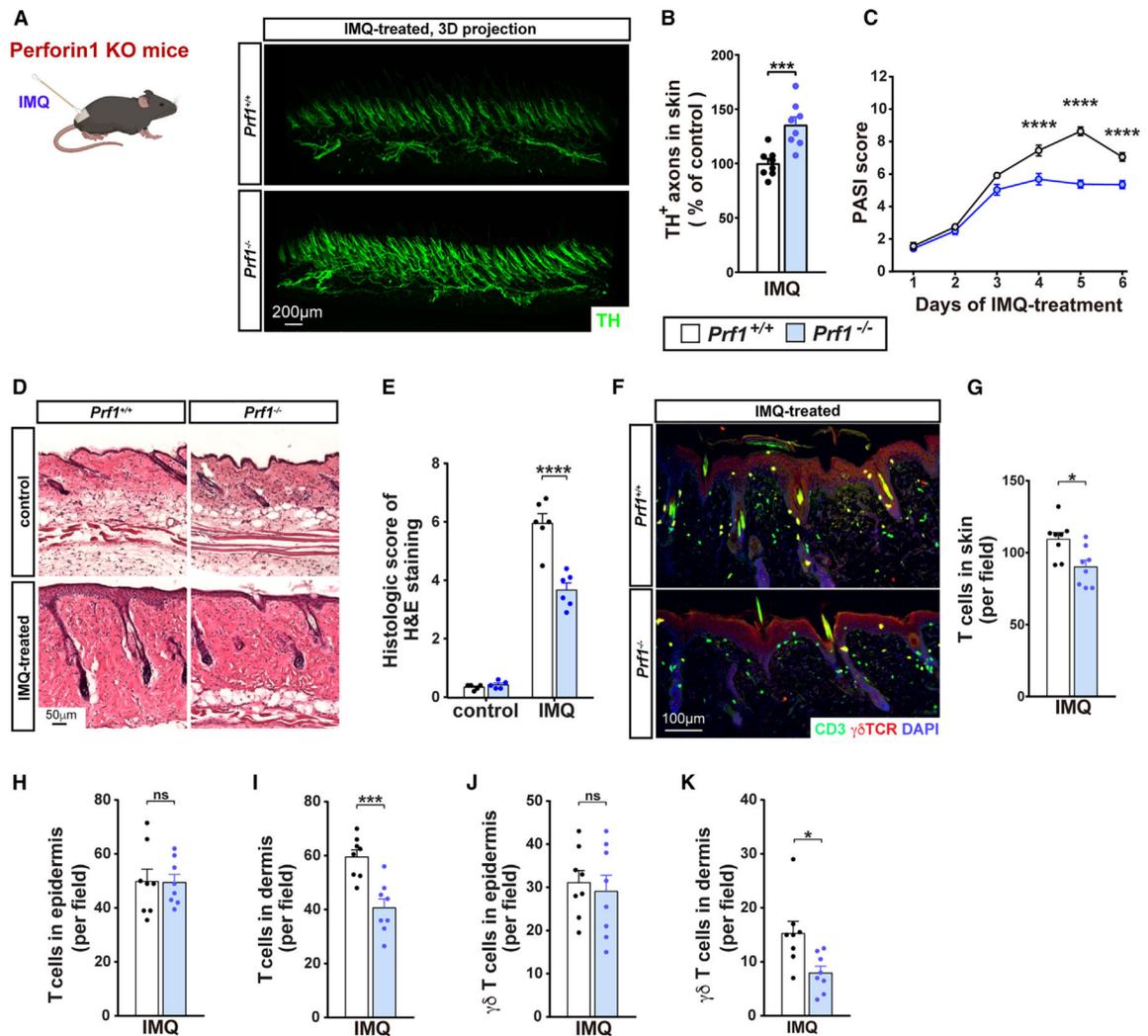
**Figure 3. Perforin-1 is required for IMQ-mediated axon loss and tissue damage**

(A and B) Mice of the indicated genotypes were subjected to 6 days of daily IMQ treatment. TH$^+$ axons were visualized at the terminal time point (A), and their number was quantified (B). n = 8 mice, mean ± SEM, unpaired, two-tailed t test.

(C) The response to IMQ was further assayed by PASI. n = 6, mean ± SEM, two-way ANOVA with Sidak's correction.

(D and E) IMQ-induced tissue damage was assessed by H&E (D) and quantified using Baker's standard (E). n = 5 (control) or 6 (IMQ), mean ± SEM, two-way ANOVA with Tukey's post hoc test.

(F) Inflammation was assessed by immunostaining in tissue sections of the indicated genotypes.

(G−K) The indicated populations were counted across each field of view at 10× magnification. Dermis and epidermis were identified by the density of the DAPI signal (F, blue channel) and differentially quantified. n = 8 mice, mean ± SEM, unpaired, two-tailed t test.

**Figure 4. TH+ axon depletion enhances IMQ-induced skin inflammation**

(A) Dorsal skin was treated with vehicle or 6-OHDA, followed by daily IMQ treatments, as indicated. Representative 3D projection of skin treated as indicated and visualized by whole-mount immunolabeling for TH.

(B) TH+ sympathetic axons were quantified. n = 5 mice, mean ± SEM, unpaired, two-tailed t test.

(C) Expression of *IL-17A* and *IL-17F* in skin was quantified by qPCR at the terminal (day 6) time point. n = 5 (control) or 9 (IMQ), mean ± SEM, two-way ANOVA with Tukey's post hoc test. A similar analysis was performed to measure IL-17A and IL-17F proteins in Figure S5B.

(D and E) Representative images of the H&E-stained skin sections from the indicated conditions (D), quantified in (E). n = 5, mean ± SEM, two-way ANOVA with Tukey's post hoc test.

(F) PASI of mouse dorsal skin was evaluated every day before IMQ treatment. n = 9 mice, mean ± SEM, two-way ANOVA with Sidak's correction.

(G) CD45+ CD3+ γδ TCR+ IL-17A+ cells in the skin tissue were quantified by flow cytometry. n = 9 mice, mean ± SEM, unpaired, two-tailed t test. The gating strategy is presented in Figure S5A.

**Figure 5. Blocking TH+ axon degeneration lessens IMQ-induced skin inflammation**
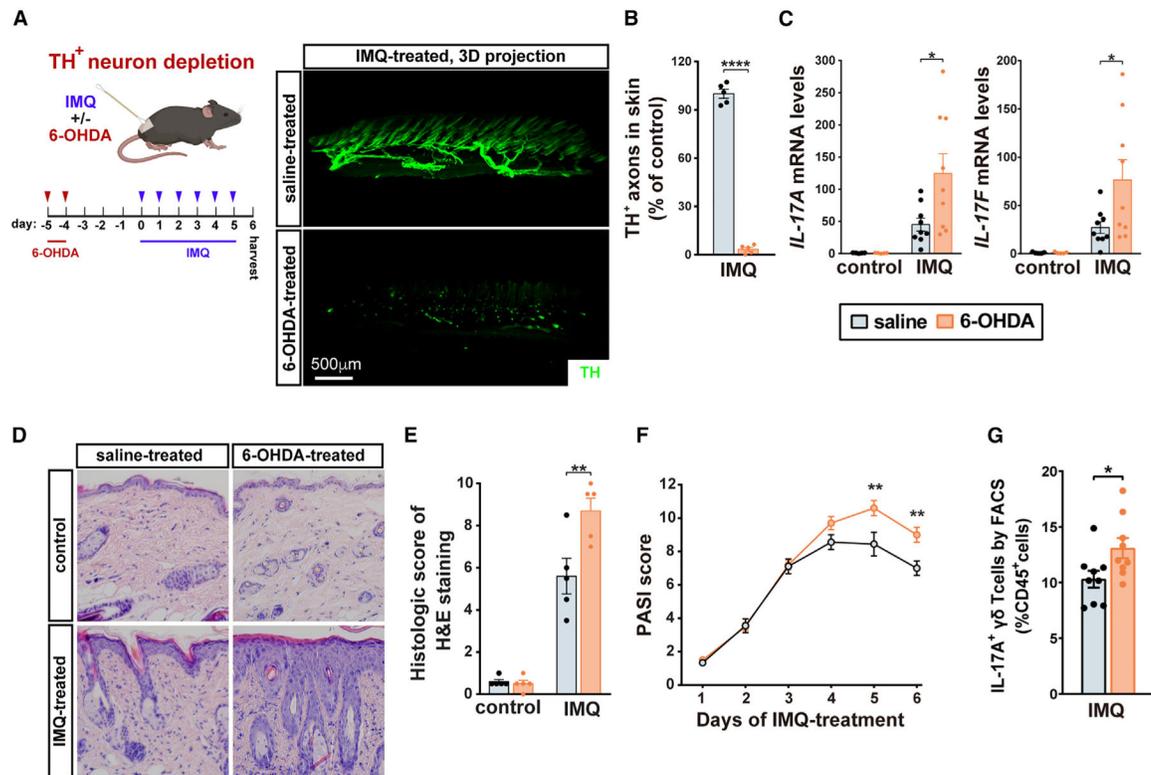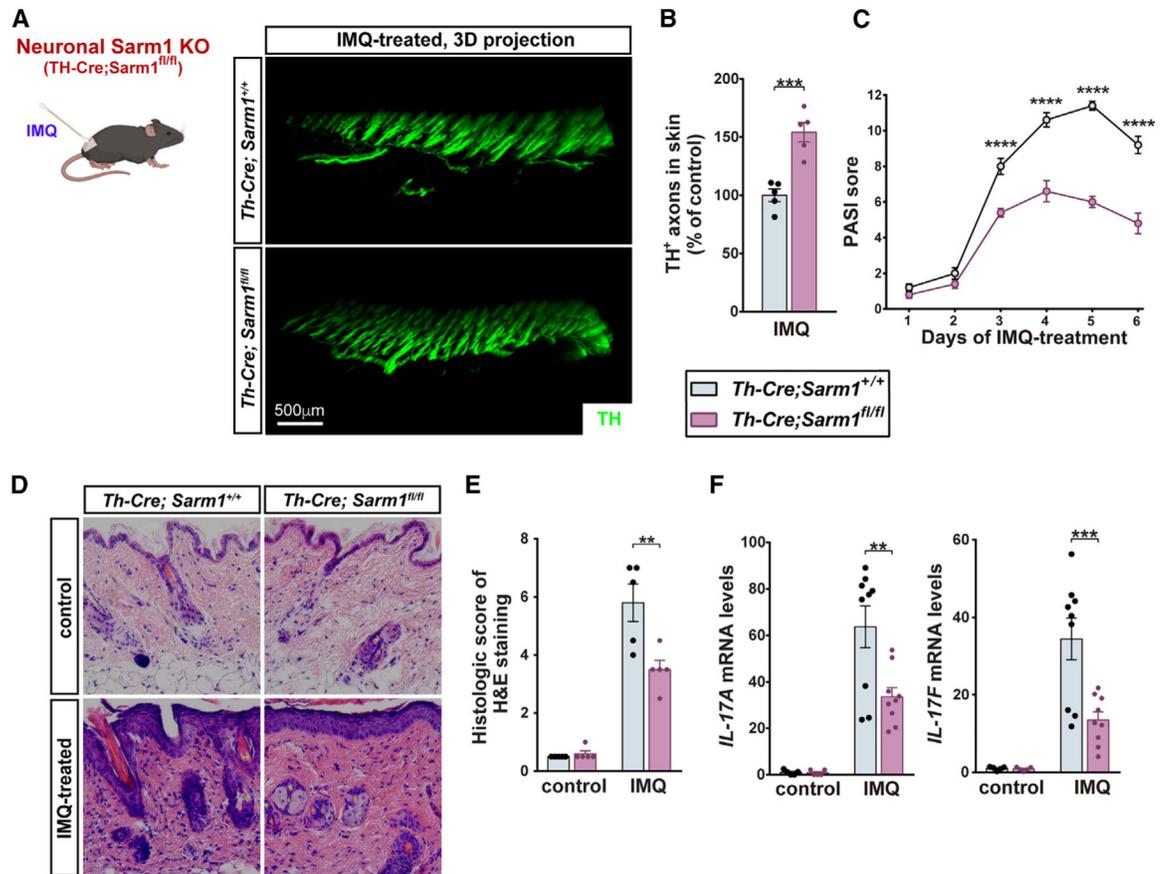
(A and B) Mice of the indicated genotypes were subjected to 6 days of daily IMQ treatment. TH+ axons were visualized at the terminal time point (A), and their density was quantified (B). n = 5 mice, mean ± SEM, unpaired, two-tailed t test.

(C) The response to IMQ was further assayed by PASI. n = 5 mice, mean ± SEM, two-way ANOVA with Sidak's correction.

(D and E) IMQ-induced tissue damage was assessed by H&E (D) and quantified using Baker's standard (E). n = 5 mice, mean ± SEM, two-way ANOVA with Tukey's post-hoc test.

(F) Expression of *IL-17A* and *IL-17F* in skin was quantified by qPCR. n = 5 (control) or 9 (IMQ), mean ± SEM, two-way ANOVA with Tukey's post hoc test.
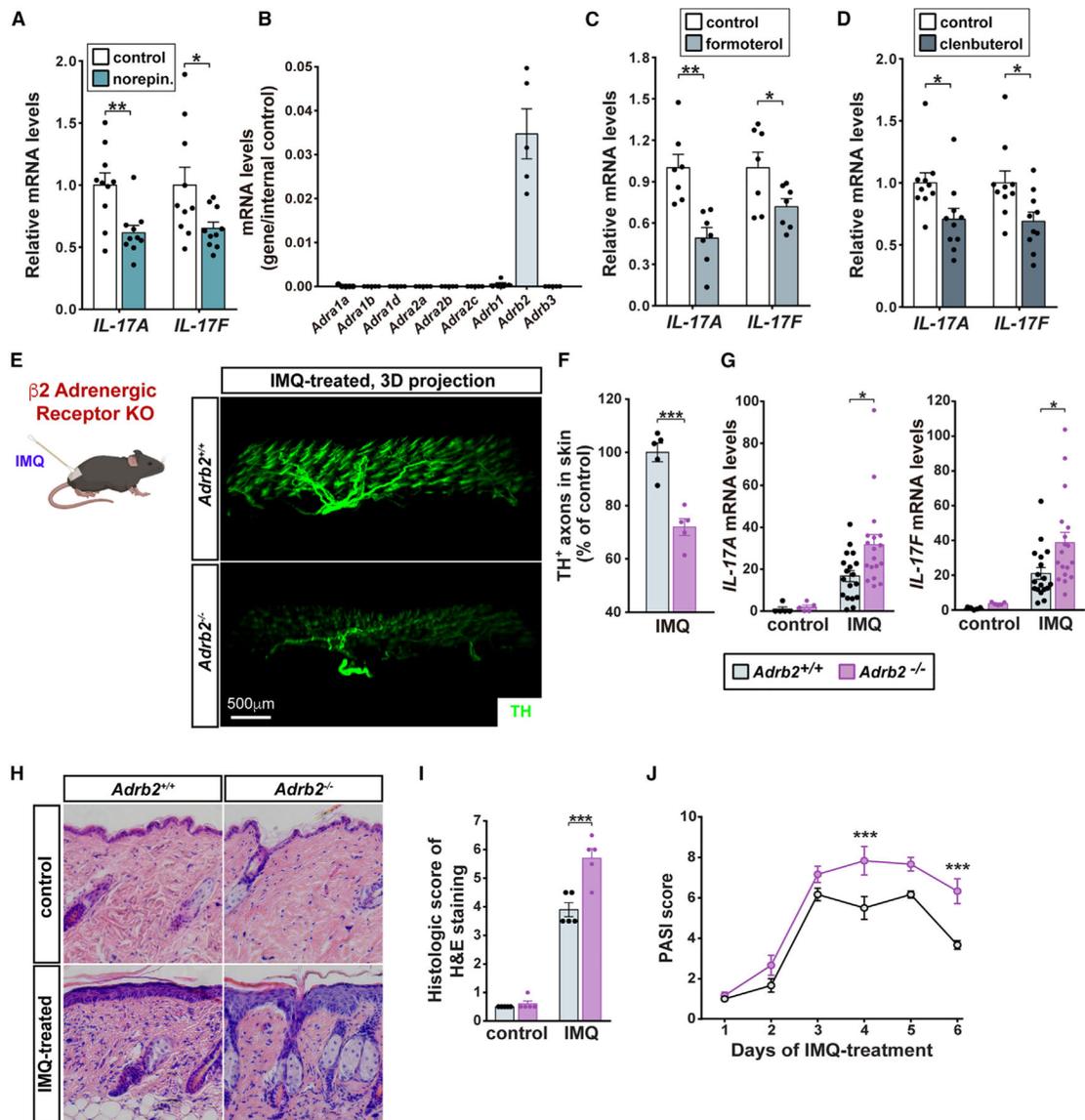
**Figure 6. A norepinephrine (NE)-β2 adrenergic receptor signaling axis lowers skin inflammation**

(A) γδ T cells (CD45^{+} CD3^{+} γδ TCR^{+}) isolated from subcutaneous lymph nodes of IMQ-treated wild-type mice were treated with 20 μM NE, followed by expression analysis of indicated genes. n = 10 mice, mean ± SEM, unpaired, two-tailed t test.

(B) The expression profile of adrenergic receptors in γδ T cells was determined by qPCR. n = 5 mice, mean ± SEM.

(C and D) γδ T cells were treated with 20 μM of the indicated drugs followed by expression analysis. n = 7 (formoterol) or 10 (clenbuterol), mean ± SEM, unpaired, two-tailed t test.

(E and F) Representative 3D-projection images of 1-mm-thick IMQ-treated skin sections of the indicated genotypes (E). TH[+] axon density is quantified in (F). n = 5 mice, mean ± SEM, unpaired, two-tailed t test.

(G) Expression of *IL-17A* and *IL-17F* in skin was determined by qPCR. n = 5 (control) or 18 (IMQ), mean ± SEM, two-way ANOVA with Tukey's post hoc test.

(H and I) IMQ-induced tissue damage was assessed by H&E (H) and quantified using Baker's standard (I). n = 5 mice, mean ± SEM, two-way ANOVA with Tukey's post hoc test. (J) The response to IMQ was further assayed by PASI. n = 6 mice, mean ± SEM, two-way ANOVA with Sidak's correction.
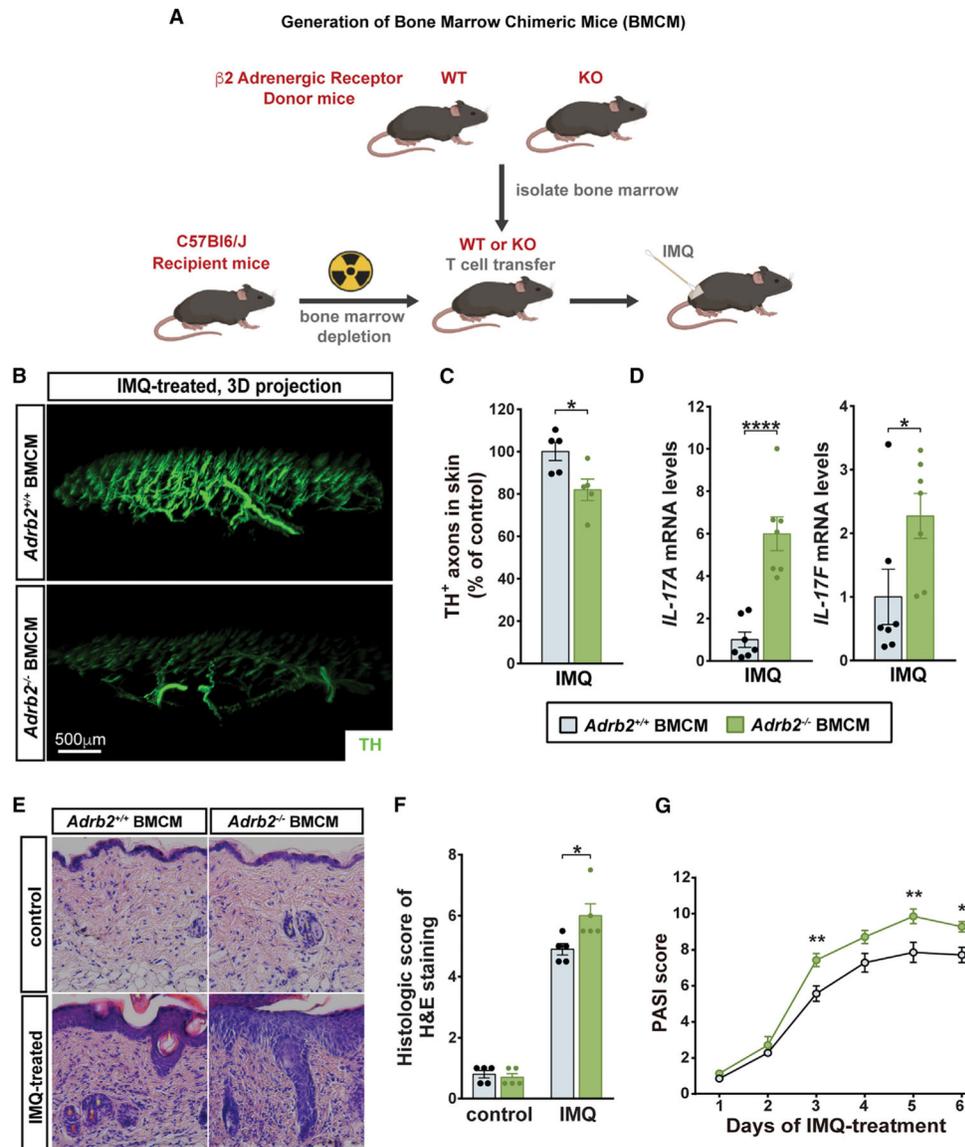
**Figure 7. β2 adrenergic receptor acts in the immune compartment to limit IMQ-induced inflammation**

(A) Schematic of bone marrow transplantation to generate Adrb2 chimeric mice. Wild-type recipient mice were irradiated to deplete endogenous bone marrow and subsequently injected with $2 \times 10^6$ bone marrow-derived cells from donor mice ($Adrb2^{+/+}$ or $Adrb2^{-/-}$) via intravenous injection.

(B and C) Bone marrow chimeric mice (BMCMs) were treated with IMQ (B), and TH$^+$ axon number was quantified (C). n = 5 mice, mean ± SEM, unpaired, two-tailed t test.

(D) Expression level of *IL-17A* and *IL-17F* in skin was determined by the qPCR. n = 7 mice, mean ± SEM unpaired, two-tailed t test.

(E and F) Skin samples from the indicated conditions were processed for H&E staining (E), and histologic scores were determined using Baker's standard (F). n = 5, mean ± SEM, two-way ANOVA with Tukey's post hoc test.

(G) The response to IMQ was further assayed by PASI. n = 7 mice, mean ± SEM, two-way ANOVA with Sidak's correction.

KEY RESOURCES TABLE

| REAGENT or RESOURCE | SOURCE | IDENTIFIER |
| --- | --- | --- |
| Antibodies | | |
| Anti-Mouse PGP9.5 | ProteinTech Group | RRID:AB_2210497 |
| Anti-Mouse Tyrosine Hydroxylase | Millipore | RRID:AB_390204 |
| Anti-Mouse CD45 PE-Cy7 | Biolegend | RRID: AB_312979 |
| Anti-Mouse CD3 Brilliant Violet 421 | Biolegend | RRID: AB_10900227 |
| Anti-Mouse CD3 PE | Biolegend | RRID: AB_312663 |
| Anti-Mouse γδ TCR FITC | Biolegend | RRID: AB_313830 |
| Anti-Mouse IL17A APC | eBioscience | RRID: AB_763580 |
| Donkey anti-Rabbit IgG (H + L) Highly Cross-Adsorbed Secondary Antibody, Alexa Fluor 647 | Invitrogen | RRID: AB 2536183 |
| Donkey anti-Chicken IgY (H + L) Highly Cross Adsorbed Secondary Antibody, Alexa Fluor 647 | Invitrogen | RRID: AB_2921074 |
| Donkey anti-Rabbit IgG (H + L) Highly Cross-Adsorbed Secondary Antibody, Alexa Fluor 790 | Invitrogen | RRID: AB_2534145 |
| Donkey anti-Rat IgG (H + L) Highly Cross-Adsorbed Secondary Antibody, Alexa Fluor 568 | Invitrogen | RRID: AB 2910653 |
| Goat anti-Armenian Hamster IgG (H + L) Highly Cross-Adsorbed Secondary Antibody, Alexa Fluor 647 | Invitrogen | RRID: AB_2925790 |
| InVivoMAb anti-mouse CD8α | BioXCell | Cat: BE0004- |
| InVivoMAb anti-mouse TCR γ/δ | BioXCell | Cat: BE0070 |
| InVivoMAb rat IgG2a isotype control | BioXCell | Cat: BE0089 |
| InVivoMAb polyclonal Armenian hamster IgG | BioXCell | Cat: BE0091 |
| Fc Block | eBioscience | RRID: AB_468582 |
| Chemicals, peptides, and recombinant proteins | | |
| Imiquimod Cream | Padagis Israel Pharmaceuticals Ltd | N/A |
| 6-Hydroxydopamine (6-OHDA) | Sigma-Aldrich | Cat: 162957-50MG |
| Nair Hair Removal Lotion | Church & Dwight Co., Inc. | N/A |
| PrimeScript RT Reagent Kit | Takara | Cat: RR047A |
| PowerUp SYBR Green Master Mix for qPCR | Thermo Fisher Scientific | Cat: A25742 |
| Dispase II | Sigma Aldrich | Cat: D4693-1G |
| Collagenase IV | Sigma-Aldrich | Cat: V900893 |
| Hyaluronidase | Sigma-Aldrich | Cat: H3884-100MG |
| DNAse I | Sigma-Aldrich | Cat: D5025-15KU |
| Phorbol-12-Myristate-13-Acetate | Santa Cruz Biotechnology | Cat: sc-3576 |
| Ionomycin | MP Biomedicals Inc | Cat: 02155070-CF |
| Norepinephrine | Sigma-Aldrich | Cat: A7256-1G |
| Formoterol | Sigma-Aldrich | Cat: F9552 |
| Clenbuterol | Sigma-Aldrich | Cat: C5423 |
| Ascorbic acid | Sigma-Aldrich | Cat: A92902-25G |
| TRIzol | Thermo Fisher Scientific | Cat: 15596026 |

| REAGENT or RESOURCE | SOURCE | IDENTIFIER |
|---|---|---|
| Critical commercial assays | | |
| IL-17A Elisa Kit | MEIMIAN | Cat: MM-0759M1 |
| IL-17F Elisa Kit | MEIMIAN | Cat: MM-1129M1 |
| Experimental models: Organisms/strains | | |
| Mouse: C57BL6/J | The Jackson Laboratory | RRID:IMSR JAX:000664 |
| Mouse: *Th-Cre* | The Jackson Laboratory | RRID:IMSR_JAX:008601 |
| Mouse: *Adrb1*$^{-/-}$ *Adrb2*$^{-/-}$ | The Jackson Laboratory | RRID:IMSR_JAX:003810 |
| Mouse: *Sarm1*$^{-/-}$ | The Jackson Laboratory | RRID:IMSR_JAX:018069 |
| Mouse: *Prf1*$^{-/-}$ | The Jackson Laboratory | RRID:IMSR_JAX:002407 |
| Mouse: *Tcrbd*$^{-/-}$ | The Jackson Laboratory | RRID:IMSR_JAX: 002122 |
| Mouse: Sarm1$^{fl/fl}$ | Jing Yang Lab, Peking University | Sun et al. 2021[30] |
| Mouse: *Tcrd-H2B-eGFP* | The Jackson Laboratory | RRID:IMSR_JAX: 016941 |
| Oligonucleotides | | |
| Mouse Cyclophilin Q-PR F: TGGAGAGCACCAAGACAGACA | Integrated DNA Technologies | This paper |
| Mouse Cyclophilin Q-PR R: TGCCGGAGTCGACAATGAT | Integrated DNA Technologies | This paper |
| Mouse IL17A Q-PCR F: CAGGGAGAGCTTCATCTGTGT | Integrated DNA Technologies | This paper |
| Mouse IL17A Q-PCR R: GCTGAGCTTTGAGGGATGAT | Integrated DNA Technologies | This paper |
| Mouse IL17F Q-PCR F: CCCAGGAAGACATACTTAGAAGAAA | Integrated DNA Technologies | This paper |
| Mouse IL17F Q-PCR R: GCAAGTCCCAACATCAACAG | Integrated DNA Technologies | This paper |
| Software and algorithms | | |
| Imaris | Bitplane | https://imaris.oxinst.com/packages |
| Prism | GraphPad | https://www.graphpad.com/scientific-software/prism |
| FlowJo | FlowJo | https://www.flowjo.com |
| ImageJ | ImageJ | https://imagej.net/ij/ |
| SOAPNuke | Github | https://github.com/BGI-flexlab/SOAPnuke |